Journal of Power Sources xxx (2009) xxx–xxx

Contents lists available at ScienceDirect

Journal of Power Sources

journal homepage: www.elsevier.com/locate/jpowsour

Tradeoffs between battery energy capacity and stochastic optimal power management in plug-in hybrid electric vehicles☆

Scott J. Moura[a,*], Duncan S. Callaway[b], Hosam K. Fathy[a], Jeffrey L. Stein[a]

[a] Department of Mechanical Engineering, University of Michigan, Ann Arbor, MI, United States
[b] Energy and Resources Group, University of California, Berkeley, CA, United States

ARTICLE INFO

Article history:
Received 27 August 2009
Received in revised form 4 November 2009
Accepted 5 November 2009
Available online xxx

Plug-in hybrid electric vehicles
Lithium ion batteries
Power management
Stochastic dynamic programming
Optimal control
Battery sizing

ABSTRACT

Recent results in plug-in hybrid electric vehicle (PHEV) power management research suggest that battery energy capacity requirements may be reduced through proper power management algorithm design. Specifically, algorithms which blend fuel and electricity during the charge depletion phase using smaller batteries may perform equally to algorithms that apply electric-only operation during charge depletion using larger batteries. The implication of this result is that "blended" power management algorithms may reduce battery energy capacity requirements, thereby lowering the acquisition costs of PHEVs. This article seeks to quantify the tradeoffs between power management algorithm design and battery energy capacity, in a systematic and rigorous manner. Namely, we (1) construct dynamic PHEV models with scalable battery energy capacities, (2) optimize power management using stochastic control theory, and (3) develop simulation methods to statistically quantify the performance tradeoffs. The degree to which blending enables smaller battery energy capacities is evaluated as a function of both daily driving distance and energy (fuel and electricity) pricing.

1. Introduction

This article examines plug-in hybrid electric vehicles (PHEVs), which utilize onboard battery storage to displace liquid fuels with less expensive grid electricity. Battery sizing and design play key roles in the cost, reliability, and ability of PHEVs to effectively manage different power demand levels over the course of a diverse set of trip durations [1]. The goal of this article is to examine the how PHEV operating cost is influenced by battery energy capacity and power management algorithm design. We specifically focus on quantifying the extent to which different PHEV power management algorithms enable the use of smaller batteries without compromising performance and efficiency. This quantification focuses on two power management algorithms: the first, which has been used in several preceding studies, minimizes fuel consumption by aggressively depleting battery charge when it is available. As in preceding work, we will refer to this algorithm as charge-depletion-charge-sustenance (CDCS). The second algorithm simultaneously combines fuel and electricity usage to minimize total operating costs, and as such is referred to as a "blended" approach. The performance and efficiency characteristics of these algorithms are compared for different battery sizes over stochastic distributions of drive cycle trajectories and trip durations.

The hybrid electric vehicle powertrain control and design literature contains two relevant, occasionally overlapping bodies of research: power management control design and battery sizing studies. Within the power management body of research, investigators have generally considered two types of control algorithms: trajectory-based and static feedback-based methods. Trajectory-based algorithms seek to synthesize optimal control input trajectories given some knowledge of the drive cycle. Deterministic dynamic programming methods require exact knowledge of the drive cycle *a priori* [2–4], while model predictive control techniques estimate drive cycle power demand online [5]. Static feedback-based methods seek to synthesize a function that maps the PHEV plant state variable values to the control inputs, using heuristic rules [6,7], parametric optimization [8], or stochastic dynamic programming [9–13], to name a few examples. It should be noted that, with the exception of [9], these studies develop control strategies that seek to minimize gasoline consumption, rather than total vehicle operating costs.

In the area of battery sizing, researchers often attempt to determine the appropriate battery design parameters given some combination of PHEV model, drive cycle, and power management strategy. For example, in lifecycle cost/energy policy-focused

☆ Based on "Impact of Battery Sizing on Stochastic Optimal Power Management in Plug-in Hybrid Electric Vehicles", by Scott J. Moura, Duncan. S. Callaway, Hosam K. Fathy, Jeffrey L. Stein, which appeared in *Proceedings of the 2008 IEEE International Conference on Vehicular Electronics and Safety*, Columbus, OH, © 2008 IEEE.

* Corresponding author. Tel.: +1 734 763 7388; fax: +1 734 764 4256.
E-mail addresses: sjmoura@umich.edu (S.J. Moura), dcal@berkeley.edu (D.S. Callaway), hfathy@umich.edu (H.K. Fathy), stein@umich.edu (J.L. Stein).

0378-7753/$ – see front matter © 2009 Elsevier B.V. All rights reserved.
doi:10.1016/j.jpowsour.2009.11.026

Nomenclature

a	error between sample and population means
b	probability of error a between population and sample means
A_{fr}	PHEV front cross sectional area (m^2)
C	trip cost random variable (USD)
C_d	PHEV air drag coefficient
F	reaction force b/w sun and planet gears (N)
F_{drag}	viscous air drag force (N)
F_{road}	PHEV road loads (N)
F_{roll}	rolling friction force (N)
$f(x, u)$	PHEV dynamics function
$g(x, u)$	cost per time step (USD s^{-1})
$I'_{M/G2}$	effective motor/generator 2 inertia (PHEV + M/G2) ($N\,m^2$)
J	optimization objective (USD)
k	discrete time index (s)
K	final drive gear ratio
m_{cell}	battery cell weight (kg)
$m_{chassis}$	PHEV chassis weight (w/o battery pack) (kg)
$m_{pack,nom}$	nominal battery pack weight (kg)
m_{veh}	total PHEV weight (kg)
n	number of iterations for simulation method
N	optimal control problem time horizon (s)
n_s	number of battery pack cells configured in series per string
n_p	number of parallel strings in battery pack
P_{batt}	battery pack power demand (W)
$P_{chg,lim}$	battery pack charging power limit (W)
$P_{dis,lim}$	battery pack discharging power limit (W)
P_{dem}	drive cycle power demand (W)
p_{ijm}	transition probability for Markov chain model
Q	battery pack charge capacity (Ah)
Q_{cell}	battery cell charge capacity (Ah)
R, S	number of teeth on ring and sun gears, respectively
R	battery pack internal resistance (Ω)
R_{cell}	battery cell internal resistance (Ω)
SOC	battery pack state of charge (Ah Ah^{-1})
T_e	engine torque (N m)
$T_{M/G1}$	motor/generator 1 torque (N m)
$T_{M/G2}$	motor/generator 2 torque (N m)
$T'_{M/G2}$	effective motor/generator 2 torque (Road loads +M/G2) (N m)
u	PHEV control input vector
V_{oc}	battery pack open circuit voltage (V)
$V_{oc,cell}$	battery cell open circuit voltage (V)
v	PHEV longitudinal velocity ($m\,s^{-1}$)
W_{fuel}	engine fuel consumption rate ($g\,s^{-1}$)
x	PHEV state variable vector

Greek letters

α_{elec}	electricity W to MJ s^{-1} conversion factor
α_{fuel}	fuel $g\,s^{-1}$ to MJ/s^{-1} conversion factor $\left(\frac{\text{MJ<CE:HSP SP="0.25"/>s}^{-1}}{\text{g<CE:HSP SP="0.25"/>s}^{-1}}\right)$
β	energy price ratio $\left(\frac{\text{USD MJ}^{-1}}{\text{USD MJ}^{-1}}\right)$
γ	discount factor
μ	rolling friction coefficient
ρ	air density ($kg\,m^{-3}$)
Φ	cumulative density function for $N(0, 1)$ random variable
ω_e	engine crankshaft speed (rad s^{-1})
$\omega_{M/G1}$	motor/generator 1 speed (rad s^{-1})
$\omega_{M/G2}$	motor/generator 2 speed (rad s^{-1})

studies, researchers attempt to determine the appropriate battery energy capacity that would render PHEVs economically competitive [14,15]. In drive cycle requirement-type studies, researchers assume knowledge of the PHEV model and power management strategy and then calculate the required battery power and energy requirements to complete a given drive cycle [6,16–18]. In control-oriented battery sizing studies, researchers assume knowledge of the PHEV model and drive cycle, and then determine the appropriate control strategy to complete a given drive cycle for various battery designs [3,6,7]. One key conclusion of this literature is that operating PHEVs in an all-electric battery depletion mode often requires batteries with both high energy and high power characteristics, thus resulting in more expensive components [6,7,16–18]. This motivates the use of smaller batteries in combination with control strategies that reduce electric power requirements by shifting load to the combustion engine.

This article links the PHEV power management and battery sizing literature by examining the influence of battery energy capacity on the performance of optimal control strategies in a single mode power-split PHEV. We build directly upon our previous work [9], in which we developed PHEV models and optimal control strategies using stochastic dynamic programming. In that work we found that, for a PHEV design with a 4 kWh capacity, the optimal control strategy blends gasoline with electric power even when the battery state of charge is high and power demand is below the capacity of the electric drivetrain. This result is in contrast to other PHEV power management research [6–8], which focuses on aggressively depleting battery charge if the energy is available, and uses blending only to reduce battery power requirements. However, the performance differences between blending and aggressive charge depletion is generally a strong function of battery energy capacity, drive cycle duration, and energy purchase prices. This fact motivates the results reported in the present article.

The original contributions of this article are three-fold. First, this is the first study of which we are aware that examines the question of how battery energy capacity influences optimal PHEV control strategies. We find that a blended control strategy is particularly effective at reducing operating costs for batteries with low energy capacity. A consequence of this result is that fewer battery cells are required to achieve a given cost-per-kilometer target with the blended approach. Second, because trip length plays an important role in determining the benefits of added battery energy capacity, we draw upon transportation survey data to develop trip duration distributions for evaluating control strategy performance. In general, blending provides greater performance benefits for longer trips. Finally, we investigate how the price of fuel relative to electricity influences PHEV control strategy performance for a range of battery sizes. We find that blending control is especially important when fuel prices are relatively low.

The remainder of the article is organized as follows: Section 2 introduces the vehicle configuration, PHEV model, power management algorithms, daily travel time distributions, and drive cycles. Section 3 describes the article's simulation approach. Section 4 presents the main results and discusses the impact of battery size, control strategy, daily trip distance, and energy prices on operating cost and energy consumption. The article's conclusions are provided in Section 5.

Please cite this article in press as: S.J. Moura, et al., J. Power Sources (2009), doi:10.1016/j.jpowsour.2009.11.026

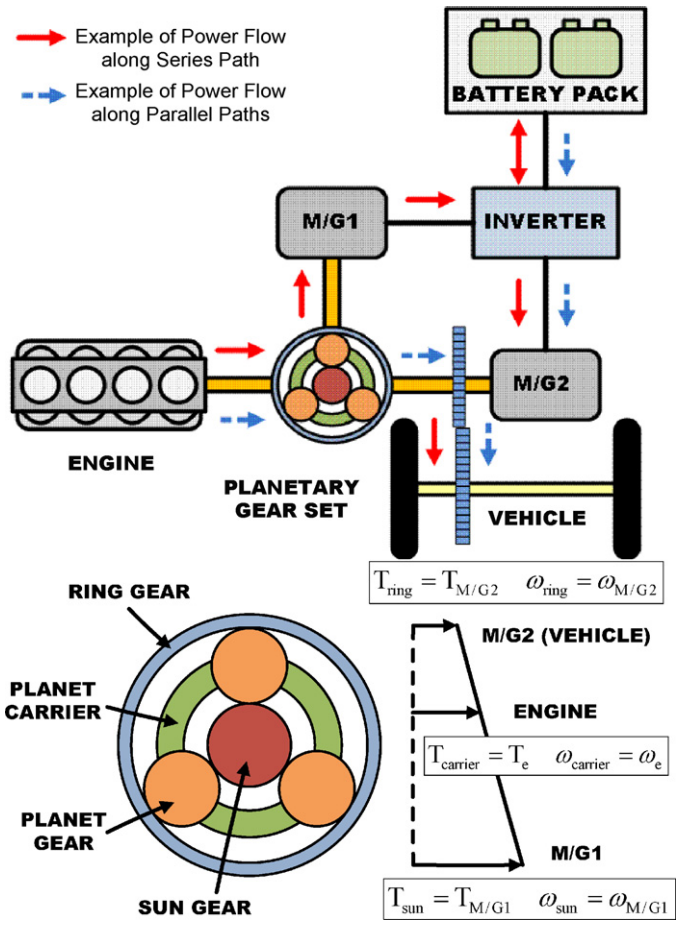

Fig. 1. The single mode power-split hybrid architecture uses a planetary gear set to split power amongst the engine, M/G1, and M/G2. Diagram adapted from [19].

Table 1
PHEV model specifications.

Vehicle	EPA classification	Midsize Sedan
	Chassis curb weight	$m_{chassis} = 1320$ kg
Engine	Type	Gasoline inline 4-cylinder
	Displacement	1.5 L
	Maximum power	43 kW at 4000 RPM
	Maximum torque	110 N m at 4000 RPM
Motor/generators	Type	Permanent Magnet AC
	M/G1 maximum power	15 kW at 3000–5500 RPM
	M/G2 maximum power	33 kW at 1040–5600 RPM
Battery pack	Cell chemistry	Lithium ion
	Nominal voltage	3.3 V per cell
	Nominal capacity	2.3 Ah per cell
	Voltage limits	2 V–3.6 V
	Battery pack nominal weight	$m_{pack,nom} = 36$ kg
	Battery cell weight	$m_{cell} = 0.07$ kg

2. Model development

This article analyzes a plug-in hybrid electric vehicle model based upon the single mode power-split (a.k.a. parallel/series or combined) hybrid architecture in Fig. 1. The key benefit of the power-split design is that it possesses energy flow characteristics of both parallel and series configurations. The parallel flow paths include engine-to-wheels and battery-to-wheels (blue dashed arrows), while the series flow path is from the engine-to-battery-to-wheels (red solid arrows). The role of the planetary gear set is to manage energy flow between these paths by transferring mechanical power between the engine, two motor/generators (identified as M/G1 and M/G2), and the wheels [19]. An appealing result of this arrangement is that, with the appropriate control strategy, power can be split amongst the three paths to optimize energy consumption. The objective of the power management algorithm developed in this article is to determine the optimal engine, M/G1, and M/G2 torque inputs as a function of the PHEV states. Here, optimality is measured with respect to expected electricity plus gasoline expenditures. In the following subsection, we provide a summary of the PHEV model used to develop the optimal power management algorithms. Parameter values and specifications for the PHEV model are provided in Table 1.

2.1. PHEV model

The PHEV model used in this article, summarized below, and described in detail in [9], builds upon existing research on conventional hybrid electric vehicles (HEVs) [2,10,11]. The vehicle model comprises five components shown schematically in Fig. 2:

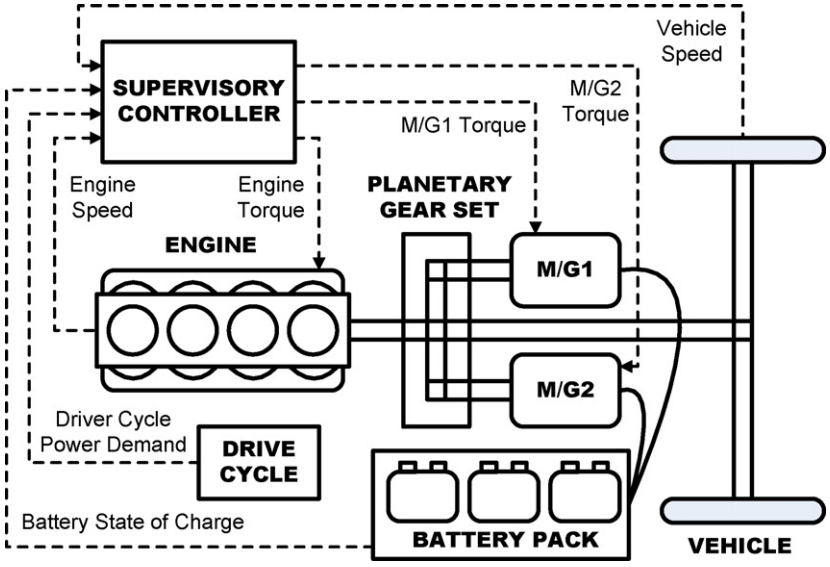

Fig. 2. PHEV model components and signal flow. Note that the signal flow forms a state feedback control architecture.

Please cite this article in press as: S.J. Moura, et al., J. Power Sources (2009), doi:10.1016/j.jpowsour.2009.11.026

Table 2
Summary of PHEV model equations [9].

State variables	$x = [\ \omega_e \quad v \quad SOC \quad P_{\text{dem}}\ ]^T$
Control inputs	$u = [\ T_e \quad T_{M/G1} \quad T_{M/G2}\ ]^T$
Inertial dynamics	$\begin{bmatrix} I_e & 0 & 0 & R+S \\ 0 & I_{M/G1} & 0 & -S \\ 0 & 0 & I'_{M/G2} & -R \\ -(R+S) & S & R & 0 \end{bmatrix} \begin{bmatrix} \dot{\omega}_e \\ \dot{\omega}_{M/G1} \\ \dot{\omega}_{M/G2} \\ F \end{bmatrix} = \begin{bmatrix} T_e \\ T_{M/G1} \\ T'_{M/G2} \\ 0 \end{bmatrix}$
	$I'_{M/G2} = I_{M/G2} + (I_w + m_{\text{veh}} r_{\text{tire}}^2)/K^2$
	$T'_{M/G2} = T_{M/G2} - F_{\text{road}} r_{\text{tire}}/K$
	$m_{\text{veh}} = m_{\text{chassis}} + m_{\text{pack,nom}} + m_{\text{cell}} n_s n_p$
Road loads	$F_{\text{road}} = F_{\text{roll}} + F_{\text{drag}}$
	$F_{\text{roll}} = \mu m_{\text{veh}} g$
	$F_{\text{drag}} = 0.5 \rho A_{\text{fr}} C_d v^2$
Battery *SOC* dynamics	$\dot{SOC} = \frac{V_{\text{oc}}(SOC) - \sqrt{V_{\text{oc}}(SOC)^2 - 4P_{\text{batt}}R}}{2QR}$
	$P_{\text{batt}} = T_{M/G1}\omega_{M/G1}\eta_{M/G1}^{k_{M/G1}} + T_{M/G2}\omega_{M/G2}\eta_{M/G2}^{k_{M/G2}}$
	where $k_i = \begin{cases} -1 & \text{if } T_i\omega_i > 0 \\ 1 & \text{otherwise} \end{cases}$ for $i = \{M/G1, M/G2\}$

the engine, motor/generators, planetary gear set, longitudinal vehicle dynamics, and battery pack. The engine and motor/generator models are steady-state maps that respectively output fuel consumption rate and power efficiency as functions of speed and torque [20]. The drive cycle is modeled as a stochastic process, which we describe in detail in Section 2.3.1. Models for the remaining components are summarized in Table 2, and can be grouped in terms of the inertial dynamics, road loads, and battery state-of-charge dynamics. The states for the assembled PHEV plant model include engine crankshaft speed ω_e, longitudinal vehicle velocity v, battery state of charge *SOC*, and driver power demand P_{dem}. The controlled inputs to the plant include engine torque T_e, M/G1 torque $T_{M/G1}$, and M/G2 torque $T_{M/G2}$. Fig. 2 shows how the state and control signals form a state feedback control loop around the PHEV model components, through the supervisory controller. The following discussion provides a high-level summary of dynamic models in Table 2; full details are available in [9].

The inertial dynamics model utilizes Euler's Law and the kinematic constraints imposed by the planetary gear set to determine the engine and motor/generator speeds [11]. Note that this model includes the longitudinal vehicle dynamics through the effective inertia $I'_{M/G2}$ and torque $T'_{M/G2}$ on M/G2. This furnishes a combination of three ordinary differential equations and one kinematic constraint, which yields two independent dynamic equations for the engine speed ω_e and forward vehicle velocity v state variables, where v is directly proportional to $\omega_{M/G2}$ through the tire radius and final drive ratio K. The road loads F_{road} act as resistive terms to the forward vehicle velocity dynamics. These loads include rolling resistance F_{roll} and viscous air drag F_{drag}.

Observe that the vehicle mass m_{veh} is scalable with respect to the number of cells in the Li-ion battery pack. Here, m_{chassis} is the PHEV weight without the battery pack, $m_{\text{pack,nom}}$ represents the nominal battery pack weight (e.g. packaging, thermal regulation hardware, power electronics, etc.) and m_{cell} is the weight of each Li-ion battery cell. As a result, the PHEV mass is an affine function of the number of Li-ion battery cells, as shown in Table 3.

Battery pack power and energy characteristics are modeled by representing each Li-ion cell as an equivalent circuit comprising an ideal voltage source $V_{\text{oc,cell}}$ in series with a resistor R_{cell} [11,21], where each cell has a charge capacity of Q_{cell}. The open circuit voltage is a function of battery state of charge (*SOC*), taken from the specification sheet provided by A123 Systems [22]. These equivalent circuits are assembled in a series-parallel combination to model the entire battery pack, where n_s denotes the number of cells in series per parallel string and n_p denotes the number of parallel strings. The total number of cells in the pack is $n_s n_p$. The open circuit voltage V_{oc}, internal resistance R, and charge capacity Q for the entire battery pack are given by:

$$V_{\text{oc}} = n_s V_{\text{oc,cell}} \tag{1}$$

$$R = \frac{n_s}{n_p} R_{\text{cell}} \tag{2}$$

$$Q = n_p Q_{\text{cell}} \tag{3}$$

In this article, we use the parameters n_s and n_p to scale the total energy capacity of the PHEV battery pack. The battery pack dynamics are associated with *SOC*, which intuitively describes a battery "fuel gauge". Here, we define *SOC* as the ratio of battery pack charge to maximum charge capacity. Through applying power conservation on the equivalent circuit, we obtain an expression for battery power at the terminals which may be solved in terms of *SOC* to obtain the ordinary differential equation for *SOC* in Table 2.

Although this formulation explicitly accounts for series-parallel cell architectures, it can be mathematically shown that, holding $n_s n_p$ constant, the *SOC* dynamics are invariant to n_s and n_p individually. We will use this fact to avoid the need to specify the cell architecture. As a result, this study considers the PHEVs with the battery energy capacities and vehicle curb weights described in Table 3. Although packaging, pack voltage, inverter efficiency, thermal management, charge equalization, and state of health are

Table 3
Battery pack energy capacities, no. of cells, and PHEV masses.

Energy capacity	No. of Li-ion cells	PHEV curb weight
2 kWh	263 cells	1374 kg
4 kWh	526 cells	1393 kg
6 kWh	789 cells	1411 kg
8 kWh	1052 cells	1430 kg
10 kWh	1315 cells	1448 kg
12 kWh	1578 cells	1467 kg
14 kWh	1841 cells	1485 kg
16 kWh	2104 cells	1503 kg

Please cite this article in press as: S.J. Moura, et al., J. Power Sources (2009), doi:10.1016/j.jpowsour.2009.11.026

factors that affect the battery design process [23,24], they are not critical to this article's investigation.

2.2. Power management algorithm

In previous work we developed optimal PHEV power management algorithms that minimize the combined cost of consuming fuel and electricity [9]. As in other work [2,10–13], these control strategies are optimized subject to a stochastic model of drive cycle power demand (described in Section 2.3.1), rather than a specific drive cycle known *a priori*. Mathematically, the optimal control problem is summarized by the following infinite horizon formulation:

$$\text{Minimize} \quad J = \lim_{N\to\infty} \mathrm{E}_{P_{\text{dem}}}\left[\sum_{k=0}^{N-1} \gamma^k g(x(k), u(k))\right] \tag{4}$$

$$\text{subject to} \quad x(k+1) = f(x(k), u(k)) \tag{5}$$

$$p_{ijm} = \Pr(P_{\text{dem}}(k+1) = i | P_{\text{dem}}(k) = j, v(k) = m) \tag{6}$$

$$\left\{ x \in \mathbb{R}^4 \;\middle|\; \begin{array}{c} \omega_{e,\min} \le \omega_e \le \omega_{e,\max} \\ \omega_{M/G1,\min} \le \omega_{M/G1} \le \omega_{M/G1,\max} \\ \omega_{M/G2,\min} \le \omega_{M/G2} \le \omega_{M/G2,\max} \\ SOC_{\min} \le SOC \le SOC_{\max} \end{array} \right\} \tag{7}$$

$$\left\{ u \in \mathbb{R}^3 \;\middle|\; \begin{array}{c} T_{e,\min} \le T_e \le T_{e,\max}(\omega_e) \\ T_{M/G1,\min} \le T_{M/G1} \le T_{M/G1,\max} \\ T_{M/G2,\min} \le T_{M/G2} \le T_{M/G2,\max} \\ P_{\text{chg,lim}}(SOC) \le P_{\text{batt}} \le P_{\text{dis,lim}}(SOC) \end{array} \right\} \tag{8}$$

$$P_{\text{dem}} = P_e + P_{M/G1} + P_{M/G2} \tag{9}$$

where (4) represents the discounted total energy consumption cost across an infinite horizon, averaged across the stochastic distribution of drive cycle power demand P_{dem}. The function $g(x(k), u(k))$ is the energy consumption cost per time step k (discussed in detail in Sections 2.2.1 and 2.2.2), and γ is the discount factor. The optimization is subject to both deterministic (5) and stochastic (6) model dynamics. The deterministic dynamics in (5) refer to the dynamic PHEV model described in Section 2.1. The stochastic dynamics (6) take the form of a first order Markov chain, described in full detail in Section 2.3.1. The set constraints of (7) and (8) represent the sets of admissible state and control values, respectively. These constraints generally represent actuator and state variable saturation limits (see [9] for details). The equality constraint in (9) is a power conservation constraint that sets the total power generated from each source equal to the drive cycle power demand. This constraint ensures the problem is well-posed in the sense that it eliminates the trivial solution of providing zero engine and electric power to minimize energy consumption cost.

Within this framework, we developed two separate control strategies, "blended" and "charge depletion, charge sustenance" (CDCS) in [9]. For completeness of presentation, we summarize these strategies here, which have the following definitions for the cost-per-time-step function $g(x, u)$.

2.2.1. Blended

The blended approach minimizes a weighted sum of fuel consumption and electric energy consumption

$$g(x, u) = \beta\alpha_{\text{fuel}} W_{\text{fuel}} + \alpha_{\text{elec}} \frac{1}{\eta_{\text{grid}}} P_{\text{batt}} \tag{10}$$

where the first term represents the fuel consumption cost and the second term represents grid electricity consumption cost.

The weighting parameter β is a tunable variable that enables us to emphasize the relative importance of consuming fuel over electricity. In [9], we proposed an economic interpretation of this variable by applying the following definition:

$$\beta = \frac{\text{USD Price of Gasoline per MJ}}{\text{USD Price of Grid Electricity per MJ}} \tag{11}$$

which we refer to as the "energy price ratio". For the initial set of results in this article we assume a fuel price ratio of $\beta = 0.8$, which corresponds to 2.76 USD per gallon of fuel, and 0.10 USD per kWh of grid electricity [25]. We will also report on the sensitivity of PHEV performance to shifts in the energy price ratio in Section 4.4.

The remainder of the variables in (10) have the following definitions: the conversion factors α_{fuel} and α_{elec} are selected to convert energy consumption from each source to common units of MJ per time step. The symbol W_{fuel} is the fuel consumption rate in terms of grams per time step, and P_{batt} is power flow through the battery, which can be calculated from the battery pack open-circuit voltage, charge capacity, and $\dot{SOC}$ according to

$$P_{\text{batt}} = -V_{\text{oc}} Q \dot{SOC} \tag{12}$$

Note that P_{batt} is positive for discharge events and negative for regeneration events. Hence, there exists a reward for regeneration that offsets the need to consume grid electricity. We estimate the electric energy consumed from the grid during the recharge process by dividing P_{batt} by a constant power electronics charging efficiency $\eta_{\text{grid}} = 0.98$.

2.2.2. Charge depletion, charge sustenance

It is common in PHEV power management research to use control laws that first prioritize battery energy consumption, until they enter a charge sustenance mode like those used by conventional HEVs [6–8]. This method, which we shall refer to as charge depletion, charge sustenance (CDCS), is implemented in the SDP framework here by setting α_{elec} in (10) equal to zero. This formulation penalizes the consumption of fuel only, therefore causing the power management algorithm to deplete electricity whenever possible. If the electric machines are capable of meeting the peak power demand of a given drive schedule, this formulation will produce an all-electric range during charge depletion. If the electric machines cannot meet power demand or sufficient *SOC* does not exist in the battery, then the CDCS algorithm requests engine power to satisfy drive cycle power demand. When the battery reaches a minimum *SOC* level, the inequality $SOC_{\min} \le SOC$ in the set constraint (7) forces the engine to provide power to sustain battery charge. This constraint, which is implemented as a quadratic saturation term, produces a charge sustenance mode that is equivalent to the implementation in [2].

2.3. Stochastic drive cycle model

The power management algorithm developed in the previous section is optimized with respect to a stochastic model of drive cycle behavior. In this article, the stochastic drive cycle model is used for control design (it defines the transition probabilities p_{ijm} in Eq. (6)), as well as for simulating closed-loop PHEV performance characteristics. These simulations are augmented with a daily trip duration model that simulates the distribution of PHEV driving time between charging events (we assume that charging occurs only once per day). The following two sections discuss these models.

2.3.1. Markov chain model for drive cycle dynamics

We model drive cycle trajectories by the following first order Markov chain in (6) and repeated here for ease of reference,

$$p_{ijm} = \Pr(P_{\text{dem}}(k+1) = i | P_{\text{dem}}(k) = j, v(k) = m) \tag{13}$$

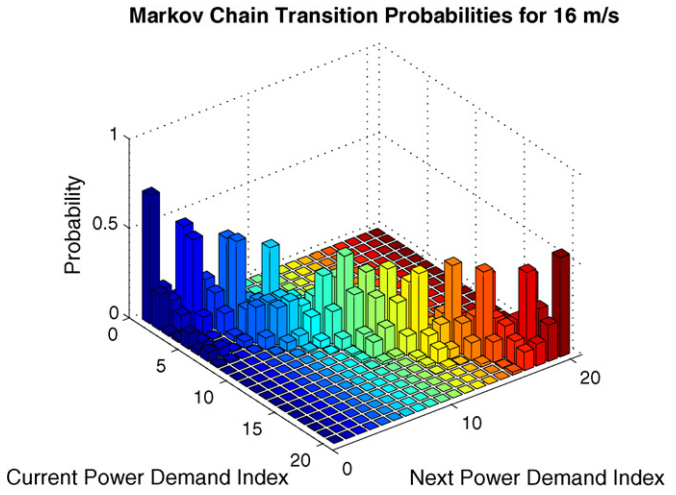

Fig. 3. Estimated drive cycle power demand transition probabilities for a vehicle velocity of 16 m s^{-1}.

where power demand P_{dem} is the Markov state variable, and p_{ijm} is the probability of power demand transitioning to level i in the next time step, given $P_{dem} = j$ and $v = m$ in the current time step. This approach to modeling drive cycle trajectories is used widely in the hybrid vehicle power management literature [2,9–13]. The transition probabilities for the Markov chain given by (13) are determined using a maximum-likelihood estimator [26] from observation data collected from federal drive cycles (FTP-72, HWFET, US06) and real-world micro-trips (WVUCITY, WVUSUB, WVUINTER) in the ADVISOR database [20]. Although the use of federal drive cycles is standard for control design and simulation, models based on naturalistic data would improve the approach. An effort to develop such models is currently underway [18] and could be easily applied to this work when complete. Fig. 3 provides an illustration of the estimated transition probabilities in the Markov chain model, for a vehicle velocity of 16 m s^{-1}. The diagonally dominant structure of the transition probabilities occurs due to the fact that power demand levels separated by one time step are highly correlated. Put simply, if the vehicle is experiencing some power demand level in the current time step, it is likely to experience a similar power demand level in the next time step.

The observation cycles and a sample randomly generated drive cycle are shown in Fig. 4. The observation cycles and randomly generated cycle produce similar characteristics. For example, the observation cycles and random cycle in Fig. 4 demonstrate average

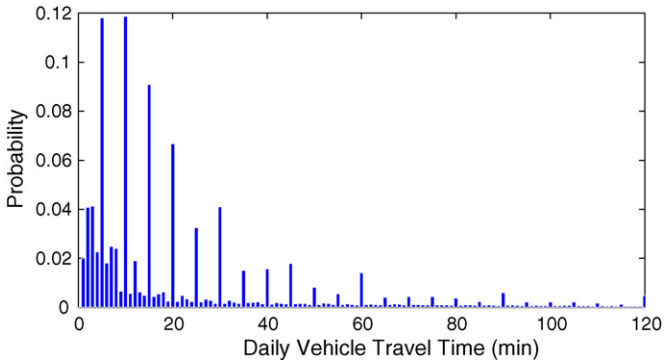

Fig. 5. Distribution of daily vehicle travel times from 2001 National Household Transportation Survey [28].

velocities of 11.7 m s^{-1} and 15.8 m s^{-1}, and maximum velocities of 35.9 m s^{-1} and 34.1 m s^{-1}, respectively.

Note that by proposing a first-order Markov chain, we assume that the drive cycles satisfy the Markov property. That is, the current state is conditioned only on the state immediately preceding it. We validated this assumption by (i) computing the residuals between the model and observation cycles, and then (ii) confirming that the autocorrelation of the residuals exceeds the 95% confidence interval for no more than 5% of all lag values—as is the case for a white noise process. This test confirms, statistically, that the drive cycles indeed satisfy the Markov property [27].

2.3.2. Trip duration model

We model trip duration as a random variable, whose distribution gives the total travel time for a vehicle during a single day, which we treat as the travel time between PHEV charging events. In this article, we construct the trip duration model from the 2001 National Household Travel Survey (NHTS) data conducted by the Department of Transportation Federal Highway Administration [28]. Fig. 5 shows the distribution of surveyed daily vehicle travel times, for which the mean is approximately 35 min and 75% of daily travel occurs in 32 min or less. The likely cause of the data's multi-modality is a tendency among survey participants to report trip duration in 5 min increments. Since our intent is to randomly generate trip durations by inverting the trip duration cumulative distribution function (cdf), we compute the cdf and attenuate the modes with a 5 min, uniformly weighted moving average in Fig. 6. Note that although we consider the NHTS data in this article, one can apply the same modeling process with any distribution of daily vehicle travel duration. Also, it is important to note that the trip

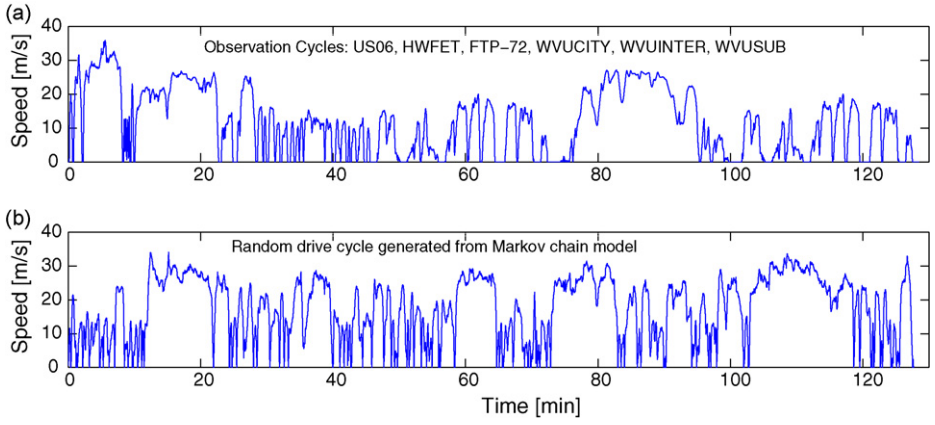

Fig. 4. (a) Observation cycles, stacked back-to-back, used to generate the Markov chain model. (b) Sample random drive cycle generated from the Markov chain model.

Please cite this article in press as: S.J. Moura, et al., J. Power Sources (2009), doi:10.1016/j.jpowsour.2009.11.026

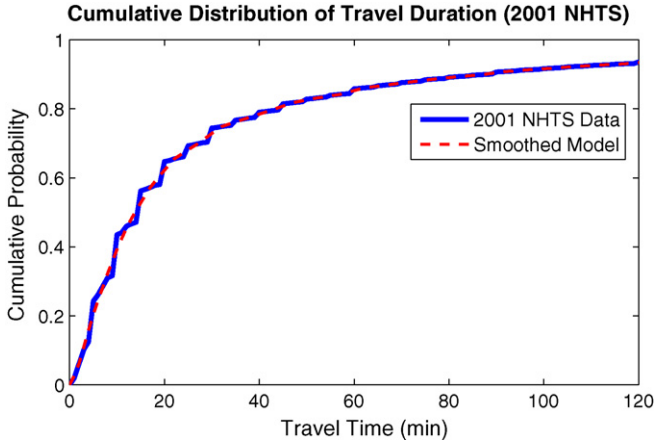

Fig. 6. Cumulative distribution of daily vehicle travel times. The smoothed model is generated by a 5 min uniformly weighted moving average of the original data.

duration model is not used during the control design process—only for closed-loop simulation and analysis.

3. Simulation method

Distributions for the PHEV performance characteristics are calculated by simulating each control strategy (Blended and CDCS) and battery size (Table 3) configuration over the entire distribution of trip duration and drive cycles. For each battery size option, we identify both a blended and CDCS control law (as explained in Section 2.2 and [9]). We then evaluate the performance of the control law/battery size combination by the following approach:

1. Generate optimal control strategies for varying battery sizes (and corresponding vehicle weights) and energy price ratios, subject to the model described in (13).
2. Generate random daily drive cycles:
   (a) Random duration—NHTS cdf shown in Fig. 6.
   (b) Random velocity profile—Markov chain model.
3. Simulate the closed loop PHEV model across the distribution of random drive cycles, generated in step 2.
4. Record the distribution of performance characteristics.
5. Repeat steps 1-4 across a range of energy price ratios.

Step 5, which obtains performance characteristics across a range of energy price ratios, furnishes the data presented in Section 4.4.

4. Results and discussion

The results from the simulation method described in the previous section enable us to analyze the coupling between battery size and control strategy. Specifically, our aim is to quantify how control strategy choice enables the use of smaller battery sizes, in terms of both operating cost and energy consumption. To facilitate this analysis, we first discuss the fundamental differences between the control strategies under investigation: blending and CDCS. Secondly, we analyze the coupling of control strategy and battery energy capacity in terms of two PHEV performance metrics: operating cost and energy consumption. Third, we consider how daily driving duration (that is, the driving time between PHEV recharge events), affects PHEV performance. Finally, Section 4 closes with an analysis of control strategy/battery size coupling as a function of the energy price ratio.

4.1. Control strategies

The key advantage of blending relative to CDCS is blending reduces the time spent in costly charge sustenance mode. This property can be understood by examining the engine operating points on a brake specific fuel consumption map for each strategy, shown in Fig. 7.

In a power-split architecture the engine is decoupled from the wheel, which enables the electric machines to move the engine operating point to regions where fuel efficiency is maximized. The optimal operating line is identified by the dashed black line in Fig. 7. During charge depletion, blending operates at low speeds near the optimal operating line. This strategy applies non-zero engine torque even when power demand can be met by the electric machines alone, where the excess power goes to regenerating battery charge, which the blended cost function (10) rewards. Once the vehicle enters charge sustenance phase, the electric machines are generally not saturated and thus free to maintain engine at relatively low speeds and high fuel efficiency.

In contrast, the CDCS approach applies zero engine torque during charge depletion, where fuel consumption is low but so is fuel efficiency. Upon entering charge sustenance, engine power is requested only when the electric machines saturate. During these periods, the electric machines lose control authority to move the engine operating point to the optimal operating line. The impact of these characteristics is that charge sustenance becomes extremely expensive, since it limits the power-split architecture's key advantage. That is, it disallows decoupling between the wheels and driver power demand.

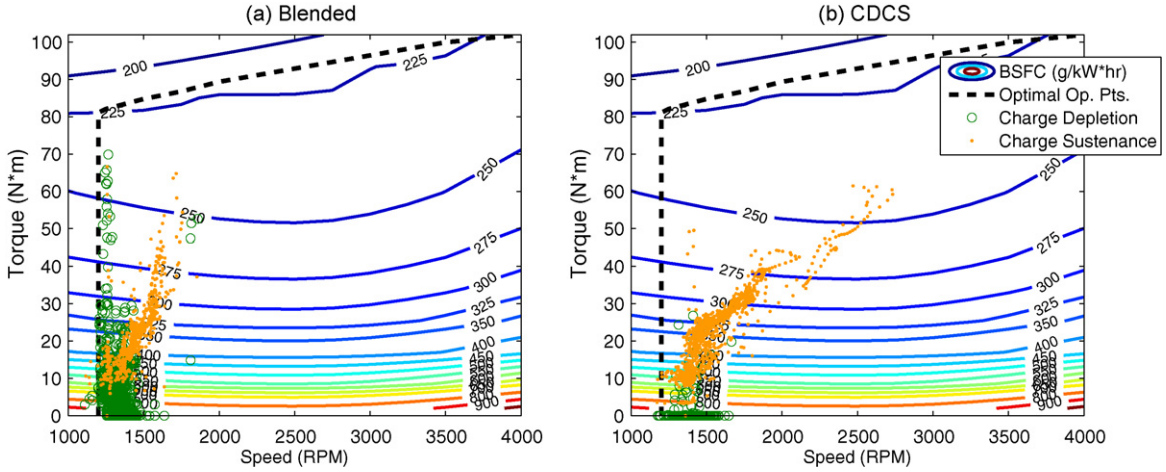

Fig. 7. Engine operating points for the (a) blended and (b) CDCS strategies on a brake specific fuel consumption map, for two FTP-72 cycles simulated back-to-back.

Please cite this article in press as: S.J. Moura, et al., J. Power Sources (2009), doi:10.1016/j.jpowsour.2009.11.026

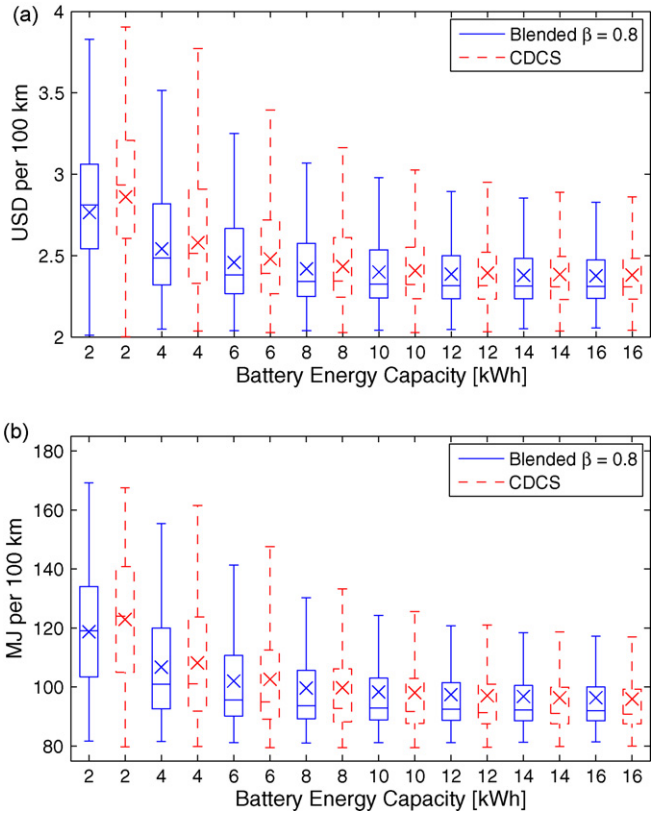

Fig. 8. Box and whisker plots of (a) operating cost (USD per 100 km) and (b) energy consumption (MJ per 100 km) distributions for each battery size and control strategy configuration. The symbol (×) denotes the average value of each distribution. Whisker lengths are limited to 1.5 times the interquartile range.

4.2. Operating cost and energy consumption

Fig. 8(a) and (b) respectively depict the distributions of operating cost (USD per 100 km) and energy consumption (MJ per 100 km) across a range of battery energy capacities. The operating cost includes both the cost of fuel from the pump, and electricity from the grid necessary to recharge the battery to its initial *SOC* level. The distributions are represented by box and whisker plots, where the (×) symbol denotes the distribution average and the whiskers are limited to 1.5 times the interquartile range.

For each battery size we observe that the distribution of operating costs and energy consumption for the blended strategy is consistently better or approximately equal to the CDCS distributions. Moreover, the advantages of blending appear to be more pronounced as battery energy capacity decreases. This can be explained by noting that as battery energy capacity decreases, the probability of fully depleting the battery on a given trip increases for either strategy. This fact is important because, as discussed in [9], blending's key advantage is that it increases the time required to fully deplete the battery. This reduces the time spent in costly charge sustenance mode, where the engine is forced out of its sweet spot in order to satisfy drive cycle power demand and regulate the battery *SOC*. Since the two strategies are roughly cost-equivalent during the charge depletion phase, the differences between them are most prevalent on cycles that force CDCS into charge sustenance mode for a significant period of time. In contrast, for large battery energy capacities, the percentage of trips which fully deplete the battery is relatively small for either strategy. Hence, the two strategies produce almost equivalent performance characteristics for large battery energy capacities.

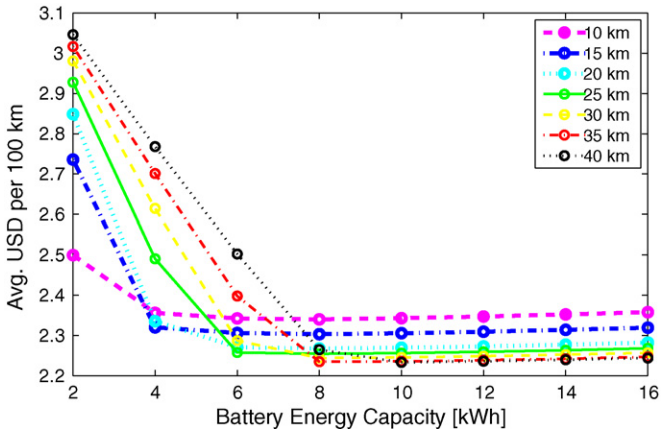

Fig. 9. Average operating cost (USD per 100 km) for varying daily trip distances and battery energy capacities, for the blended strategy.

These results are in agreement with prior claims that a blended strategy should enable the use of smaller batteries [6,7,16], although in this case the result applies to battery energy capacity, whereas the prior claims are predominantly in reference to battery power capacity. Moreover, this work justifies those claims in a more rigorous manner by developing blending strategies through optimal control theory. Furthermore, the differences between blending and CDCS are evaluated across a distribution of drive cycle behavior and daily trip times, instead of fixed drive cycles.

4.3. Impact of varying daily trip distance

This section focuses on the performance of both control strategies across varying daily trip lengths. Namely, we seek to answer the following two questions: (1) Given a fixed daily trip distance, what battery capacity minimizes energy costs? (2) For what range of trip distances does blending provide the greatest improvements over CDCS? The simulation framework used to answer these questions has one important difference with the preceding section: random drive cycles are simulated for a finite set of trip distances, as opposed to randomly sampled daily trip durations from the distribution described in Section 2.3.2.

Given a finite set of trip distances, the average operating cost as a function of battery energy capacity is demonstrated in Fig. 9, for the blended control strategy. Note that the average is taken over a set of random drive cycles generated by the Markov chain in Section 2.3.1 (where the simulation is terminated at the specified distance). For each trip distance, operating cost performance is a convex function of battery energy capacity. That is, performance decreases as battery energy capacity increases, up to a critical energy capacity. Beyond this energy capacity, operating cost increases slightly with storage capacity. This slight increase is because vehicle efficiency declines with added battery weight, which is essentially unused for the given trip distance.

The results analyzed in the preceding paragraph can also be leveraged to investigate the relative advantages of blending over CDCS across varying daily trip distances. Fig. 10 provides the percentage improvement in average operating cost performance of applying a blended strategy over CDCS. In general, blending demonstrates the greatest improvements for small battery energy capacities and long trips—up to 5%. This is because blending rations electric energy storage rather than applying aggressive depletion. The range of battery energy capacity for which blending provides an advantage over CDCS increases as trip distance increases. However, beyond a certain battery size, there is a small probability that either strategy will fully deplete the battery and therefore differ-

Please cite this article in press as: S.J. Moura, et al., J. Power Sources (2009), doi:10.1016/j.jpowsour.2009.11.026

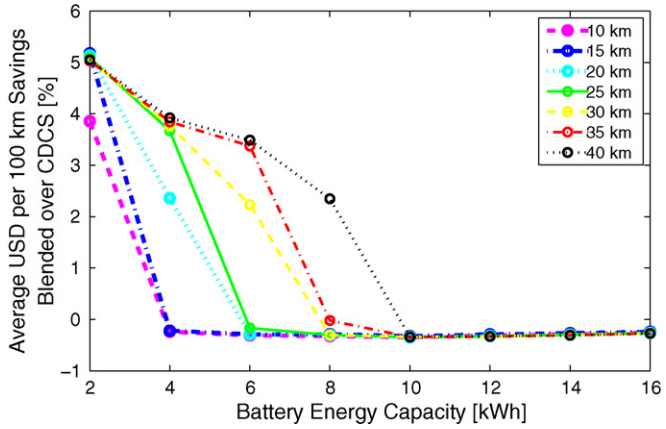

Fig. 10. Impact of daily trip distance on operating cost savings of applying a blended strategy relative to CDCS.

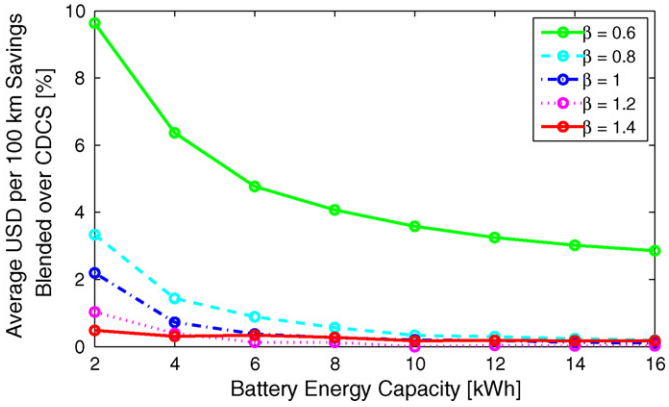

Fig. 12. Impact of energy price ratio on operating cost savings of applying a blended strategy relative to CDCS. Recall the definition of energy price ratio provided in (11).

ences between blended control and CDCS are small. In fact, for large batteries blending provides slightly worse performance than CDCS because blending applies more engine power during charge depletion to conserve electric energy. Nevertheless, Fig. 10 is useful for understanding the ranges of trip distances and battery energy capacities where blending provides significant benefits over the standard CDCS control strategy.

4.4. Impact of varying energy prices

To this point we have reported results corresponding to an energy price ratio of $\beta = 0.8$ (equivalent to the gasoline price per gallon being 27.6 times the electricity price per kWh—for example, 2.76 USD per gallon of fuel and 0.10 USD per kWh of electricity). This parameter is explicitly accounted for in both the control design procedure and simulation results. However, this value varies both temporally (e.g., by year) and spatially (e.g., by geographic region). To highlight the volatility of this parameter, consider the history of average energy price ratios in the United States since 1973 [25], shown in Fig. 11. The value of β has clearly changed significantly over the past 35 years due to shifts in both oil and electricity prices. This motivates the need to understand how this parameter impacts the interdependency of optimal power management and battery energy capacity.

Consider the operating cost savings (given in terms of percentage) of applying a blended strategy over CDCS in Fig. 12. Since the proposed simulation method produces a distribution of operating cost savings for each energy price ratio, Fig. 12 provides the average values calculated across all the drive cycles.

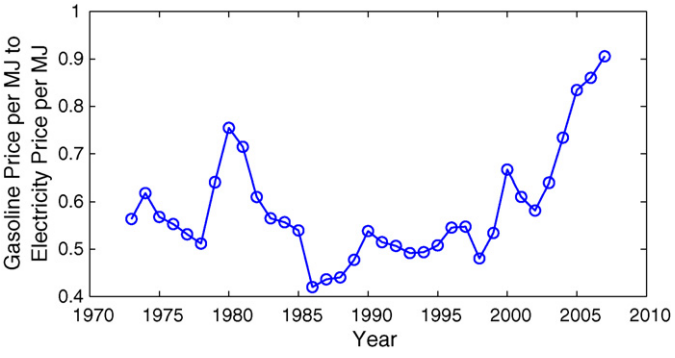

Fig. 11. Historic values for the energy price ratio β from 1973 to 2007 [25]. Note how the variation corresponds with shifts in oil and electricity prices.

Two key observations are made from the results depicted in Fig. 12. First, the benefits of blending over CDCS is more significant for smaller battery energy capacities, across all values of the energy price ratio. This result matches the trends identified in the previous section and quantifies the benefits across varying energy price ratios. Secondly, the benefits of applying a blended strategy over CDCS become notably more significant for smaller values of β, i.e. as fuel becomes less expensive relative to fixed electricity prices. This result makes intuitive sense for the following reason: recall that the blended approach explicitly accounts for the cost of fuel *and* electricity, and therefore optimally mixes these energy sources in a manner that minimizes total energy consumption costs. In the case of decreasing values for the energy price ratio, blending utilizes increasing amounts of engine power and fuel. As a result, the optimal fuel/electricity mix deviates further from the CDCS strategy, which always attempts to consume electric battery energy first. The final result is that blending produces significantly lower operating cost values relative to CDCS for small energy price ratios.

5. Conclusion

This article introduced a method for evaluating the relationships between power management strategies, battery energy capacity, daily trip distance, and energy prices in PHEVs over a distribution of drive cycle behavior and daily travel time. Through this framework, we have demonstrated several results for the single mode power split vehicle architecture. The first of these is that a blended control strategy facilitates the use of smaller batteries for a given operating cost or energy consumption level. We have also shown that expected operating cost and energy consumption approach asymptotic values as battery size increases, since a very small population of drivers will fully deplete large batteries in one day. Moreover, the benefits of blending over CDCS become more significant as trip distances increase and the energy price ratio decreases. Finally, for the case of large battery energy capacities, short trip distances, and large energy price ratio values, there exists a small penalty for applying a blended strategy over CDCS that is offset once the PHEV enters charge sustenance mode.

Acknowledgement

The authors wish to thank the National Science Foundation for financially supporting this work under the Graduate Research Fellowship Program.

References

[1] A. Simpson, Proceedings of 22nd International Battery, Hybrid and Fuel Cell Electric Vehicle Symposium and Exhibition (EVS-22), Yokohama, Japan, NREL/CP-540-40485 (2006).
[2] C.-C. Lin, Modeling and control strategy development for hybrid vehicles, Ph.D. Thesis, Department of Mechanical Engineering, University of Michigan, Ann Arbor, MI, 2004.
[3] M.P. O'Keefe, T. Markel, Proc. 22nd International Battery, Hybrid and Fuel Cell Electric Vehicle Symposium, (EVS-22), Yokohama, Japan, 2006.
[4] Q. Gong, Y. Li, Z.-R. Peng, IEEE Transactions on Vehicular Technology 57 (6) (2008) 3393–3401.
[5] A. Vahidi, A. Stefanopoulou, H. Peng, IEEE Transactions on Control Systems Technology 14 (6) (2006) 1047–1057.
[6] P.B. Sharer, A. Rousseau, S. Pagerit, P. Nelson, in: Proc. 2007 SAE World Congress, SAE Paper 2007–01-0295, 2007.
[7] P.B. Sharer, A. Rousseau, D. Karbowski, S. Pagerit, in: Proc. 2008 SAE World Congress, SAE Paper 2008–01-0460, 2008.
[8] A. Rousseau, S. Pagerit, D. Gao, Plug-in hybrid electric vehicle control strategy parameter optimization, Tech. Rep., Electric Vehicle Symposium-23, 2007.
[9] S.J. Moura, H.K. Fathy, D.S. Callaway, J.L. Stein, in: Proceedings of the 2008 ASME Dynamic Systems and Control Conference, 2008.
[10] E.D. Tate, Techniques for hybrid electric vehicle controller synthesis, Ph.D. Thesis, Department of Electrical Engineering and Computer Science, University of Michigan, Ann Arbor, MI, 2007.
[11] J. Liu, H. Peng, IEEE Transactions on Control Systems Technology 16 (6) (2008) 1242–1251.
[12] I. Kolmanovsky, I. Siverguina, B. Lygoe, Proceedings of 2002 American Control Conference 2 (2002) 1425–1430.
[13] L. Johannesson, M. Asbogard, B. Egardt, IEEE Transactions on Intelligent Transportation Systems 8 (1) (2007) 71–83.
[14] D.M. Lemoine, D.M. Kammen, A.E. Farrell, Environmental Research Letters, 3 (2008) 014003 (10 pp).
[15] C.S.N. Shiau, C. Samaras, R. Hauffe, J.J. Michalek, Energy Policy 37 (7) (2009) 2653–2663.
[16] T. Markel, A. Simpson, IEEE Vehicle Power and Propulsion Conference, 2005, p. 6.
[17] A.F. Burke, Proceedings of the IEEE 95 (4) (2007) 806–820.
[18] R. Patil, B. Adornato, Z. Filipi, SAE World Congress, SAE Paper 2009-01-2715, Detroit, MI, 2009.
[19] K. Muta, M. Yamazaki, J. Tokieda, in: Proc. 2004 SAE World Congress, SAE Paper 2004–01-0064, 2004.
[20] K.B. Wipke, M.R. Cuddy, S.D. Burch, IEEE Transactions on Vehicular Technology 48 (6) (1999) 1751–1761.
[21] V.H. Johnson, Journal of Power Sources 110 (2) (2002) 321–329.
[22] A123 Systems, High Power Lithium Ion ANR26650M1 Data Sheet, 2006.
[23] M. Verbrugge, E. Tate, Journal of Power Sources 126 (1–2) (2004) 236–249.
[24] G.L. Plett, Journal of Power Sources 134 (2) (2004) 252–261.
[25] Annual Energy Review, Tech. Rep. DOE/EIA-0384, U.S. Department of Energy, 2007. http://www.eia.doe.gov/aer/.
[26] T.W. Anderson, L.A. Goodman, Annals of Mathematical Statistics 28 (1) (1957) 89–110.
[27] P.J. Brockwell, R.A. Davis, Time Series: Theory and Methods, Springer, New York, NY, 1998.
[28] National Household Travel Survey, Tech. Rep., U.S. Department of Transportation, Federal Highway Administration, 2001. http://nhts.ornl.gov/index.shtml.

Please cite this article in press as: S.J. Moura, et al., J. Power Sources (2009), doi:10.1016/j.jpowsour.2009.11.026